On the Capabilities and Limitations of Predictive, Multi-Zone Combustion Models for Hydrogen-Diesel Dual Fuel Operation

Stefan Tüchler[a,*], Pavlos Dimitriou[b]

[a] *Powertrain and Vehicle Research Centre (PVRC), Department of Mechanical Engineering, University of Bath, Claverton Down, Bath BA2 7AY, United Kingdom*
[b] *Renewable Energy Research Center, National Institute of Advanced Industrial Science and Technology (AIST), 2-2-9, Machiikedai, Koriyama, Fukushima 963-0298, Japan*

Abstract

Compared with traditional hydrocarbon fuels, hydrogen provides a high-energy content and carbon-free source of energy rendering it an attractive option for internal combustion engines. Co-combusting hydrogen with other fuels offers significant advantages with respect to thermal efficiency and carbon emissions.

This study seeks to investigate the potential and limitations of multi-zone combustion models implemented in the GT-Power software package to predict dual fuel operation of a hydrogen-diesel common rail compression ignition engine. Numerical results for in-cylinder pressure and heat release rate were compared with experimental data. A single cylinder dual-fuel model was used with hydrogen being injected upstream of the intake manifold. During the simulations low (20 kW), medium (40 kW) and high (60 kW) load conditions were tested with and without exhaust gas recirculation (EGR) and at a constant engine speed of 1500 rpm. Both single and double diesel injection strategies were examined with hydrogen energy share ratio being varied from 0-57 percent and 0-42 respectively. This corresponds to a range in hydrogen air-equivalence ratios of approximately 0-0.29.

The results show that for the single-injection strategy, the model captures in-cylinder pressure and heat release rate with good accuracy across the entire load and hydrogen share ratio range. However, it appears that for high hydrogen content in the charge mixture and equivalence ratios beyond the lean flammability limit, the model struggles to accurately predict hydrogen entrainment leading to underestimated peak cylinder pressures and heat release rates. For double-injection cases the model shows good agreement for hydrogen share ratios up to 26 percent. However, for higher energy share ratios the issue of erroneous hydrogen entrainment into the spray becomes more accentuated leading to significant under-prediction of heat release rate and in-cylinder pressure.

Keywords: Hydrogen-diesel, GT-Power, Simulation, Dual-fuel combustion, Internal combustion engine

1. Introduction

Over recent decades automotive engines have come under close scrutiny with respect to their emission levels and carbon footprint. In combination with increased consumer awareness for fuel economy and sustainability, this has led to an ever increasing strive for powertrain electrification and battery or fuel cell electric vehicles. However, electric vehicles represent long-term solutions that require major expenditures for charging infrastructure. Hence, it will be decades until the internal combustion engine (ICE) will be finally phased out. Nonetheless, there are a number of options to improve thermal efficiency and reduce greenhouse gas emissions of internal combustion engines. One of these measures is to co-combust diesel fuel with gaseous fuels, such as hydrogen.

Hydrogen is an abundant element and can be generated from multiple sources, ranging from natural gas reforming, gasification using biomass or coal and water electrolysis using (renewable) energy. Although these measures are cost and energy intensive, hydrogen as an energy carrier is of particular interest for sustainable power generation in internal combustion engines. It provides high energy content and is free of carbon atoms, making it attractive for reducing CO_2, CO and particular matter (PM) emissions. Table 1 provides a comparison of the most salient features of hydrogen and diesel fuel.

Table 1: Overview of the main properties of diesel and hydrogen. Data taken from [1, 2].

Property	Unit	Diesel	Hydrogen
Carbon content (mass fraction)	[%]	86	0
Density at 1 bar and 300K	[kg/m^3]	832	0.0838
Lower heating value (LHV)	[MJ/kg]	43	120
Autoignition temperature	[K]	473	858
Min. ignition energy	[mJ]	-	0.02
Flame velocity (Φ=1)	[cm/s]	30	250-350
Flammability limits		-	0.2-7
Stoichiometric air/fuel ratio		14.5	34

*Corresponding author
Email address: S.Tuechler@bath.ac.uk (Stefan Tüchler)

Nomenclature

$\dot{m}$	Mass flow rate in kg/s
f	Mass fraction
x_b	Mole fraction
C	Multiplier
R	Energy share Ratio
S_L	Laminar flame speed in m/s
T	Temperature in K
p	Pressure in bar
Φ	Equivalence Ratio
Ψ_v	EGR rate
η_v	Volumetric efficiency
AFR	Air-to-fuel ratio
ATDC	After top dead centre
CFD	Computational fluid dynamics
DoE	Design of experiments
EGR	Exhaust gas recirculation
EXH	Exhaust gas
FKG	Flame kernel growth
HDDF	Hydrogen-diesel dual-fuel
HRR	Heat release rate
ICE	Internal combustion engine
IVC	Intake valve closing
LHV	Lower heating value
MRE	Mean relative error
MUZ	Main unburned zone
PM	Particulate matter
RMSE	Root mean squared error
SBZ	Spray burned zone
SOC	Start of combustion
SUZ	Spray unburned zone
TFS	Turbulent flame speed
TLS	Taylor length scale
TPA	Three pressure analysis
VGT	Variable geometry turbine
df	Diffusion
entr	Entrainment
ign	Ignition
pm	Premixed
ref	Reference value
s	Static
stoich	Stoichiometric
t	Total
u	Unburned

Compared with diesel, hydrogen provides almost thrice the energy per unit mass. However, this advantage is offset by its substantially lower density compromising hydrogen storage in vehicles. Hydrogen can be run over a wide range of air-to-fuel ratios (AFR) making it particularly suitable for ICE operation. In conjunction with its low energy required for ignition, it is thus possible to run on extremely lean mixtures, albeit at the cost of higher susceptibility to knocking. High flame speed and diffusivity further ensures rapid and complete combustion with the exception of low load operation where high rates of unburned hydrogen and low combustion efficiency are observed [3]. Despite knock-on effects with respect to volumetric efficiency, hydrogen addition offers potential benefits in terms of soot, CO and CO_2 emissions [4], while increased NO_x emissions can be partially compensated through exhaust gas recirculation (EGR) [5]. Further improvements in harmful emissions can be achieved through the application of biodiesel [6]. Nonetheless, implementation of hydrogen as an engine fuel is complex in compression ignition (CI) engines due to the high autoignition temperature and low cetane number, which requires combustion to be initiated through the lower autoignition diesel fuel.

There has been a significant amount of research efforts dedicated to the examination of hydrogen as a fuel for ICE ranging from CI engines [3–9] to spark-ignition (SI) engines [10–13]. While the open literature features a wide range of experimental studies on co-combustion engines of hydrogen and diesel or gasoline, there are relatively few numerical studies available. The bulk of these studies deal with three-dimensional computational fluid dynamics (CFD) simulations on the in-cylinder combustion characteristics, chemical-kinetics of hydrogen combustion and effects on pollutant gas emissions [14–19]. One-dimensional models having established themselves as invaluable tools for predicting engine operation and pollutant gas emissions on both SI and CI engines [20, 21], have not been extensively tested on hydrogen-diesel dual fuel engine operations. To the authors' knowledge there are merely two studies that address this to present [22, 23]. Ghazal [22] used the predictive dual-fuel model implemented in the one-dimensional software GT-Power to investigate the effect of both port-fuel injected hydrogen and water on a diesel engine performance. The study considered a hydrogen share ratio of 19 percent and varied engine speed as well as injection timing examining the impact on emissions. The study of Monemian [23] dealt with a

Table 2: Engine specifications for 5.2L heavy-duty engine.

Engine type	4-cylinder inline
Displacement volume in liters	5.2
Bore x stroke in mm	115 x 125
Compression ratio	17.5:1
Crank angle at ICV	-127° ATDC
Injection system	Electronically controlled common rail injection system
Fuel strategy	Diesel (direct injection) Hydrogen (port injection)

hydrogen-diesel dual fuel (HDDF) engine run at constant speed and considering hydrogen share ratios of up to 30 percent. The primary objective of the study focused on the calibration process of the multi-zone combustion model.

Both mentioned publications consider relatively low hydrogen share ratios and do not compare the model's predictive capabilities over a wider range of hydrogen share ratios and equivalence ratios. Therefore, this study seeks to address this gap, by testing the multi-zone predictive dual-fuel combustion model implemented in GT-Power over an extensive range of hydrogen share ratios taking into account the effect of variations in load, EGR rates and diesel injection strategies. To the author's knowledge this is the first time such a characterisation is reported in the open literature.

2. Methodology

This section gives a brief introduction of the engine specifications used throughout this study as well as the experimental setup and scope of testing conditions are given. After that, the GT-power model used to predict heat release rate and in-cylinder pressure is introduced followed by the approach taken for the regression model that computes laminar flame speed.

2.1. Experimental Setup

Collection of experimental data was done on a 5.2L four cylinder heavy-duty compression-ignition engine. The engine features intake throttling valve, high pressure EGR and a variable geometry turbocharger (VGT). The experimental apparatus and instrumentation is illustrated in Figure 1. The setup has been extensively discussed by Dimitriou et al.[5] and therefore only a brief report shall be given. The engine has been instrumented with pressure sensors in all four cylinders to obtain in-cylinder pressure and thus enable computation of heat release rate. Diesel is directly injected into the cylinders via a common-rail system. In addition, the engine was modified to operate in dual-fuel mode with hydrogen being port-injected upstream of the intake manifold and downstream of the turbocharger compressor intercooler. An inline air-hydrogen mixer ensures a well-premixed mixture and homogeneous distribution to the four cylinders. The main engine specifications are summarised in Table 2.

All experimental test data were collected at a constant engine speed of 1500 rpm. Hydrogen mass injection was based on the amount of hydrogen energy with respect to the total input energy (i.e. Diesel and hydrogen), referred to as hydrogen share ratio and defined as

$$R_{H_2} = 100 \frac{\dot{m}_{H_2} LVH_{H_2}}{\dot{m}_{H_2} LVH_{H_2} + \dot{m}_{Diesel} LVH_{Diesel}} \tag{1}$$

where $\dot{m}_{H2}$ and $\dot{m}_D$ denote the mass flow rates of the two fuels and LHV_{H2} and LHV_D denote the lower heating values of hydrogen and diesel, respectively. Furthermore, one can define the equivalence ratio of the hydrogen-air mixture as

$$\Phi = \frac{AFR^{stoich}_{H_2/air}}{AFR_{H_2/air}} \tag{2}$$

where $AFR_{H_2/air}$ refers to the air-to-fuel ratio of the hydrogen-air mixture and the subscript *stoich* to the stoichiometric air-to-fuel ratio, given in Table 1.

The experimental scope involves three different load conditions, namely 20 kW, 40 kW and 60 kW and energy share ratios as defined in Equation 1 ranging from 0 to 57 percent. This corresponds to a maximum equivalence ratio of approximately 0.29. Furthermore, EGR rate was varied from approximately 0 to 30 percent. Finally, diesel injection strategy was also altered from a simple single-injection strategy to a pilot- and main-injection strategy. In both cases, the injection timing was calibrated by the engine manufacturer. Table 3 provides an overview of main operating conditions considered throughout this study.

Table 3: Overview of engine test conditions for single- and double-injection of Diesel.

Single-Injection			
Load in kW	20	40	60
Engine speed in rpm	1500	1500	1500
Diesel rail pressure in bar	865	994	1150
EGR rate in percent	0-24	0-24	0-24
R_{H_2} in percent	0-56	0-57	0-47
Φ_{H_2} in percent	0-0.21	0-0.29	0-0.23
Main injection timing (ATDC)	~-6°	~-4°	~-4°
Double-Injection			
Load in kW	20	40	60
Engine speed in rpm	1500	1500	1500
Diesel rail pressure in bar	865	994	1150
EGR rate in percent	0-25	0-25	0-28
R_{H_2} in percent	0-42	0-42	0-42
Φ_{H_2} in percent	0-0.10	0-0.17	0-0.18
Pre injection timing (ATDC)	~-24°	~-25°	~-27.5° (diesel) ~-17.3° (HDDF)
Main injection timing (ATDC)	~0.8°	~0.9°	~1.3°

2.2. GT-Power

Simulations of HDDF operation were done using a single-cylinder model, as illustrated in Figure 2a, within GT-Power v2019 by Gamma Technologies, which has established itself

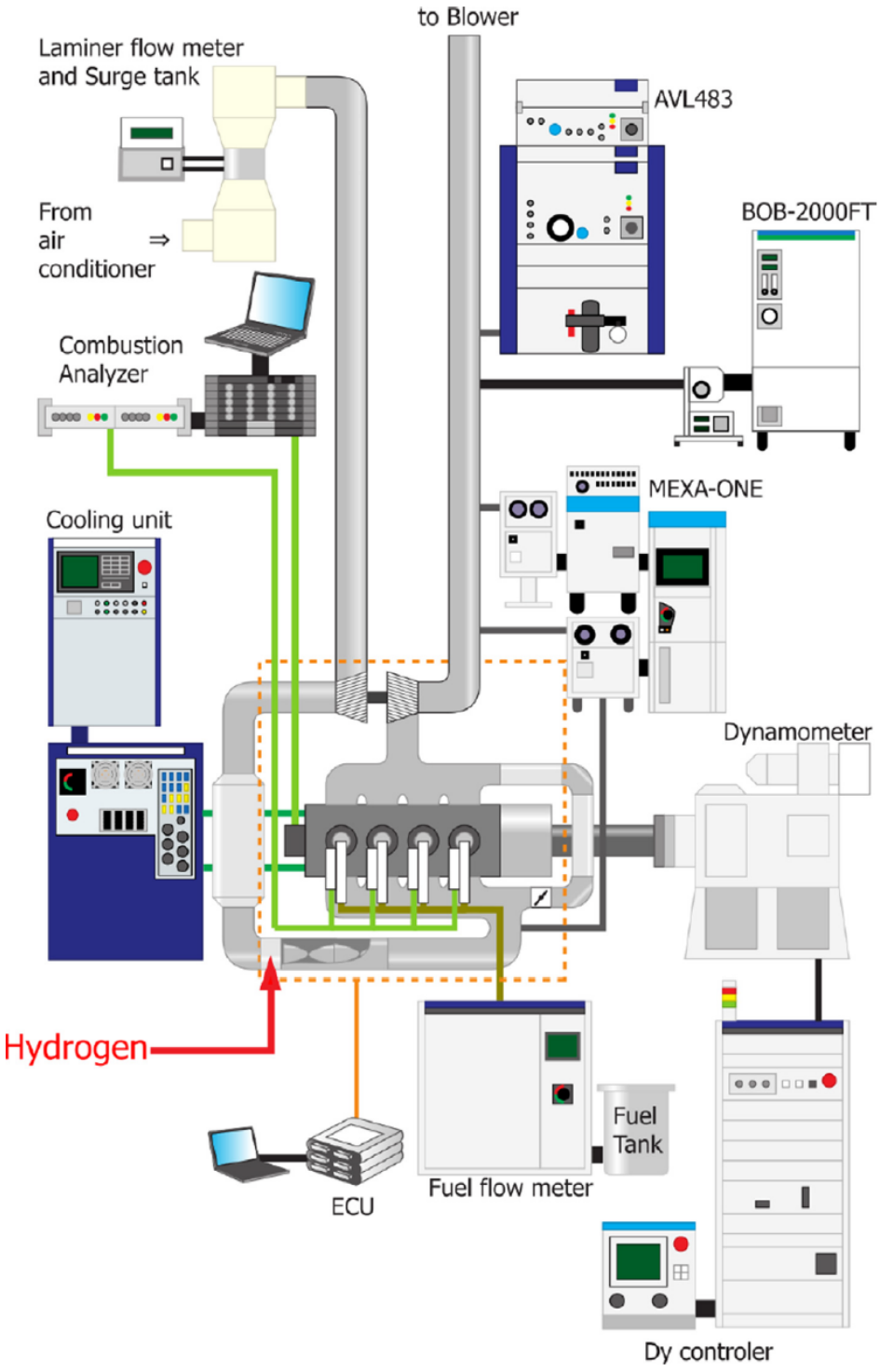

Figure 1: Overview of experimental setup including sensor locations and data acquisition system [5].

as a reliable and accurate simulation tool for combustion modelling [21]. The combustion model used throughout this study is the predictive dual fuel combustion model that employs the DIPulse combustion model for Diesel combustion and SITurb for the premixed combustion of hydrogen. The DIPulse model on the one hand follows the injected fuel, as it evaporates, entrains surrounding gases and eventually burns. It separates the combustion chamber into three thermodynamic zones; the first is the main unburned zone (MUZ), that contains all charge air at intake valve closing (IVC); the second is the spray unburned zone (SUZ), which includes injected fuel as well as entrained gases; finally, there is the spray burned zone (SBZ) that contains products of combustion.

The SITurb model on the other hand resorts to a two-zone

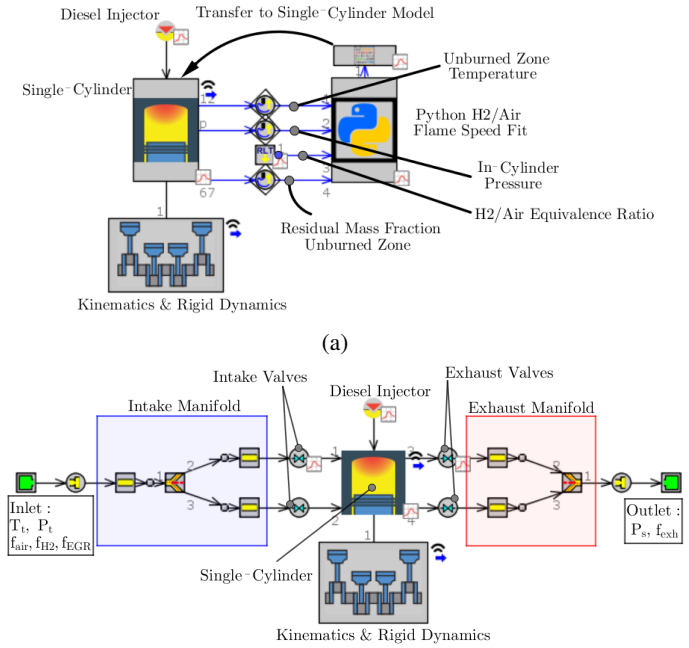

Figure 2: (a) Three pressure analysis (TPA) model used to calibrate volumetric efficiency and initialise swirl and tumble for the closed volume model given in (b), shown with Python user function to compute laminar flame speed for diesel-hydrogen dual fuel operation based on equivalence ratio, unburned zone temperature, in-cylinder pressure and residual mass fraction in the unburned zone.

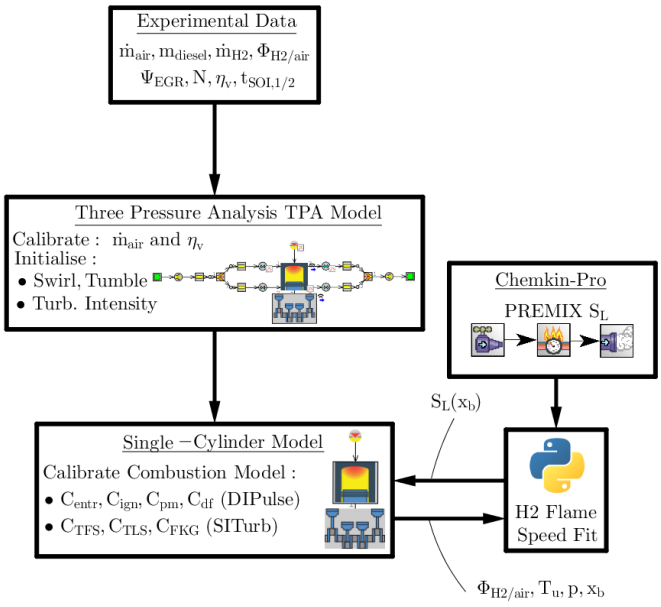

Figure 3: Flowchart outlining the calibration process for the one-dimensional simulation model. Experimental data, such as air and fuel mass flow rates, engine speed, equivalence ratios, EGR rates and injection timings are extracted and input into the three pressure analysis (TPA) model to calibrate engine breathing and initialise flow parameters within the cylinder. The final step is then calibrating DIPulse and SITurb parameters using the single-cylinder model. One-dimensional freely propagating combustion simulations using Chemkin-Pro are fed into a Python flame speed fit model implemented as a user routine within GT-Power.

model, where unburned mass is transferred from the unburned zone into the burned zone. The model includes mass entrainment of the unburned fuel and air mixtures into the flame front moving proportionally to turbulent and laminar flame speeds. The model further requires calculating laminar flame speed as a function of equivalence ratio, unburned gas temperature and pressure as well as diluent mass fraction. However, the current version of GT (v2019) significantly overestimates laminar flame speeds for hydrogen-air mixtures, even at mixtures that are beyond the flammability limit. This takes place, as GT-Power estimates laminar flame speed based on global equivalence ratio. While this approach works well with pure hydrogen combustion cases, the global equivalence ratio in dual-fuel applications is significantly different from the equivalence ratio in the unburned zone. This necessitates the generation of a user-defined regression to compute laminar flame speed based on instantaneous inputs from the model. In this instance, this was done via a Python function that transfers the computed laminar flame speed to the SITurb, overriding the original implemented model. Details of the regression model are given in the following section.

The model was setup and calibrated following the process layed out in Figure 3. Initially, experimental data from the laboratory test were extracted including mass flow rates of air, liquid and gaseous fuel, hydrogen/air equivalence ratio, EGR rate, engine speed, volumetric efficiency and injection timings. After this, a three pressure analysis (TPA) was conducted, which includes engine breathing characteristics through inclusion of intake and exhaust manifolds, as well as valves and ports. The model schematic of the TPA is given in Figure 2b. The premixed hydrogen-air charge is prescribed at the manifold inlet, while Diesel is directly injected into the cylinder. TPA ensures that conditions within the cylinder at IVC as well as swirl and tumble are accurately initialised when running the closed volume pressure analysis with the predictive combustion model. It further allows to calibrate volumetric efficiency and air mass flow rates.

With turbulence parameters and engine breathing, the next step involves calibration of the predictive combustion model done in a single-cylinder, closed volume model. The multi-zone combustion model features several parameters that can be optimised based on experimental data encompassing multipliers for entrainment rate C_{entr}, ignition delay C_{ign}, premixed combustion rate C_{pm} and diffusion combustion C_{df} (DIPulse) as well as turbulent flame speed C_{TFS}, flame kernel growth C_{FKG} and Taylor micro-scale length C_{TLS} (SITurb). These parameters are optimised using a standard elitist genetic algorithm that aims at minimising the root mean squared error between experimental and predicted heat release rate.

In case of port-injected hydrogen, a Python subroutine, which accepts values for equivalence ratio, unburned zone temperature and in-cylinder pressure, uses a fitted power-law curve to determine laminar flame speed. The data used for curve fitting was computed using the PREMIX solver in the Chemkin combustion simulation solver.

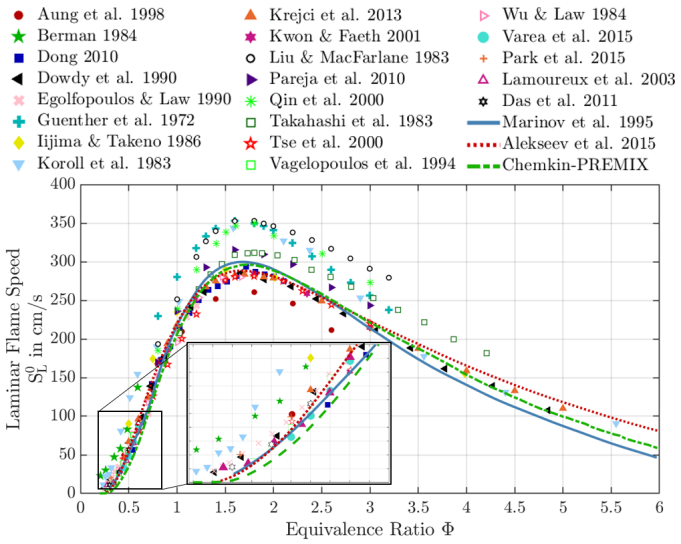

Figure 4: Comparison of experimental and literature data for laminar flame speed of hydrogen and air at ambient conditions p_0 = 1bar, T_u = 298K. The data for experimental results was taken from: Aung et al. [24], Berman [25], Dong [26], Dowdy et al. [27], Egolfopoulos and Law [28], Guenther et al. [29], Iijima and Takeno [30], Koroll et al. [31], Krejci et al. [32], Kwon and Faeth [33],Liu and MacFarlene [34], Pareja et al. [35], Qin et al. [36], Takahasi et al [37], Tse et al [38], Vagelopoulos et al. [39], Wu and Law [40], Varea et al. [41], Park et al. [42], Lamoureux et al. [43] and Das et al. [44]. Simulation results were extracted from: Marinov et al. [45] and Alekseev et al. [46]. The dash-dotted line stems from the Chemkin PREMIX model.

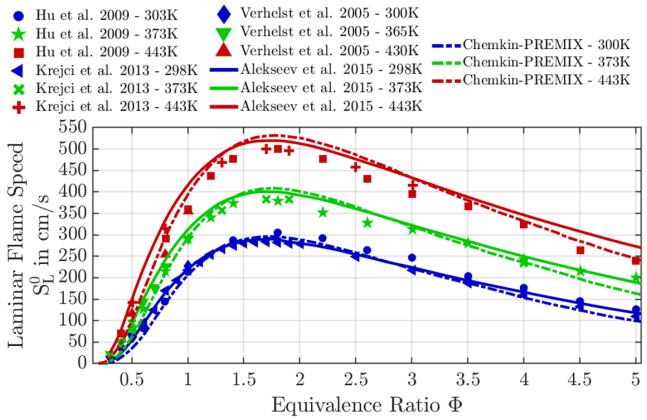

Figure 5: Comparison of experimental and literature data for laminar flame speed of hydrogen and air at elevated temperatures and ambient pressure p_0 = 1bar. The data for experimental results was taken from: Hu et al. [47], Krejci et al. [32] and Verhelst et al. [48]. Simulation results were extracted from Alekseev et al. [49]. The dash-dotted lines denote results from the Chemkin PREMIX model.

2.3. Chemkin

Modelling of premixed hydrogen-air laminar flame speeds was done in Chemkin 18.1 using the flame speed calculation model, PREMIX [50], for one-dimensional, freely propagating flames. Thermodynamic data, transport properties as well as gas-phase kinetics were evaluated using GRI-Mech 3.0 [51] chemical reaction mechanism. The model uses an implicit finite-difference approximation in steady-state to discretise balance equations for mass, momentum, energy and species. These are then solved through pseudo time-stepping to yield

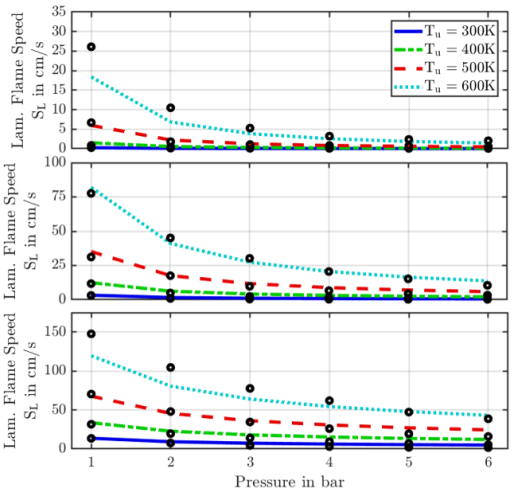

Figure 6: Laminar flame speed curve fit for elevated temperatures and pressures. Regression was done at temperatures from 300 to 600 K and pressures from 1 barA to 6 barA for three equivalence ratios at 0.25 (top), 0.325 (centre) and 0.40 (top).

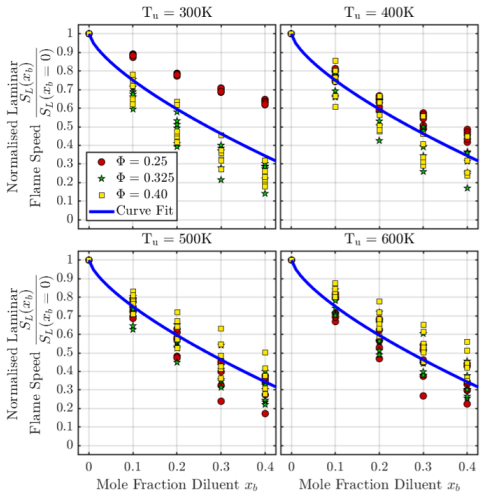

Figure 7: Effect of burned gas dilution on laminar flame speed and corresponding curve fit.

the laminar flame velocity. Throughout this study, a mixture-averaged formulation for diffusion and fluxes was chosen and the Soret effect included. Finally, an adaptive grid method was selected controlling maximum curvature and gradient ensuring zero gradients at the boundaries until convergence is obtained.

As a first step, laminar flame speeds are calculated for hydrogen-air ratios at atmospheric conditions (p_0 = 1bar, T_u = 298K) for equivalence ratios ranging from 0.2 to 6. A comparison of the resulting flame speed calculations with experimental and simulation data from the literature is given in Figure 4. The simulation data depicts trends accurately, although flame speeds tend to be slightly underpredicted with respect to the literature data. The difference to other simulation results is, however, small and discrepancies between different experiments and simulations occur as a consequence of the method used to determine flame speed and how well effects of stretch and flame curvature are reduced. As HDDF

operation predominantly occurs in the very lean region around the lower flammability limit of $\Phi = 0.2$, the focus of this study is primarily on laminar flame speeds up to an equivalence ratio of 0.4. As a result, a piece wise regression was performed yielding

$$S_{L0} = \begin{cases} -0.1239 + 6.6711(\Phi - 0.0031)^2 & \text{if } 0.20 \leq \Phi < 0.27 \\ 0.2472 + 662.0649(\Phi - 0.2575)^2 & \text{if } 0.27 \leq \Phi \leq 0.40 \end{cases} \tag{3}$$

The simulations were repeated for three different temperatures, namely at 300 K, 373 K and 447 K, while pressure was kept constant at 1 bar. The results were again compared with experimental and numerical data from the open literature and are given in Figure 5. Again, the simulation complies well with previously published simulation and laboratory data over the entire equivalence ratio range.

In order to account for the effect of higher unburned gas temperature and pressures, as will be present within the combustion chamber, a design of experiments (DoE) was conducted varying temperature in steps of 100 K between 300 and 600 K and pressure from ambient conditions (1 barA) to 6 barA. Equivalence ratio was also varied from 0.25, to 0.325 and finally to 0.4. Subsequently, a curve fit was performed following a power-law approach, as outlined by Heywood [52] and given in Figure 6.

$$\begin{aligned} S_L &= S_L^0 \left(\frac{T_u}{T_{u,ref}} \right)^{\beta_1} \left(\frac{p}{p_{ref}} \right)^{\beta_2} \\ \text{with } \beta_1 &= -11.0669 - 23.239(\Phi - 1) \\ \text{and } \beta_2 &= 3.7331 + 6.9921(\Phi - 1) \end{aligned} \tag{4}$$

Finally, the presence of burned gas in the charge as a consequence of trapped burned gas and EGR is taken into account by fitting a curve to simulation data, as given in Figure 7. The data were gathered considering unburned gas temperatures from 300 to 600 K, pressures from 1 to 6 barA and equivalence ratios in the lean region from 0.25 to 0.4. In addition, diluent mole fractions ranging from 0 to 0.4 were considered. The diluent mixture was approximated using experimental data from the exhaust manifold and included approximately 70 percent N_2, 8 percent O_2, 12 percent CO_2 and 10 percent H_2O. The final fitted curve follows Equation 5.

$$S_L(x_b) = S_L(x_b = 0)(1 - 1.2406 x_b^{0.6952}) \tag{5}$$

3. Results and Discussion

In the following section, the results for in-cylinder pressure and heat release rate obtained from GT-Power simulations are compared against the experimental data from the test bed. First of all, cases with single injection are treated. These comprise hydrogen share ratios from 0 to 56 percent and H_2-air equivalence ratios from 0 to 0.29. Thereafter, pilot injection and main injection operation is discussed with hydrogen share ratios ranging from 0 to 42 percent and H_2-air equivalence ratios from 0 to 0.18.

3.1. Single Injection

3.1.1. Diesel Operation

Figure 8 depicts data for in-cylinder pressure and heat release rate exhibiting results of both experimental and predicted model. The data encompasses low (20kW), medium (40kW) and high (60kW) load cases and variation in EGR rate as well. In addition, the annotations in the top right corner of each subplot outline hydrogen energy share ratio, equivalence ratio and EGR rate (in the format $R_{H2}/\Phi_{H_2}/\Psi_v$) for each case. To begin with, we shall first investigate how well the DIPulse model can predict diesel only operation. Therefore the test deals with 0 percent hydrogen share ratio. The dashed line outlines the start of injection not including the hydraulic delay of around 500 μs, which accounts for a delay of approximately 4.5°. At low and medium load conditions, peak heat release rate tends to be overpredicted resulting in slightly higher peak in-cylinder pressures. The relative error however remains within 5.5 percent. Towards higher loads of 60 kW start of combustion (SOC) is predicted with a delay of approximately 1°. In combination with the slightly overpredicted initial peak in heat release rate, the relative error in peak pressure reduces to less than 1 percent. In general, however, the predictive model shows good agreement with both experimental in-cylinder pressure and heat release rate for all load conditions and both high and low EGR rates, giving confidence that diesel injection and combustion are captured well. This is further emphasised when computing mean relative errors (MRE) and root mean squared errors (RMSE) between in-cylinder pressures and heat release rates (HRR) respectively, as given in Table 4.

Table 4: Mean relative error (MRE) for in-cylinder pressure and root mean squared errors (RMSE) for heat release rate between experiments and simulation for single-injection diesel-only cases with and without EGR.

	20 kW	40 kW	60 kW
p_{cyl} MRE with EGR	3.1%	1.7%	2.0%
HRR RMSE with EGR	0.0033	0.0065	0.012
p_{cyl} MRE w/o EGR	3.5%	2.1%	1.5%
HRR RMSE w/o EGR	0.0031	0.0062	0.0043

3.1.2. Hydrogen-Diesel Dual Fuel Operation

The next step involves considering hydrogen share ratios of up to 28 percent, however at equivalence ratios beyond the lower flammability limit, namely up to 0.15. As a result it can be expected that no moving flame front occurs and that all the hydrogen combustion stems from entrainment of hydrogen into the diesel spray upon injection. The flame speed model takes this into account by setting laminar flame speed to zero as soon as the equivalence ratio falls below the flammability limit of 0.2. Therefore, the characteristics in terms of pressure and heat release rate are not expected to vary dramatically. This is confirmed when inspecting Figure 8b in more detail. While heat release rate tended to be slightly overpredicted in diesel-only operation for low and medium loads, it now appears to be more in line or gently underpredicted, reducing relative error in

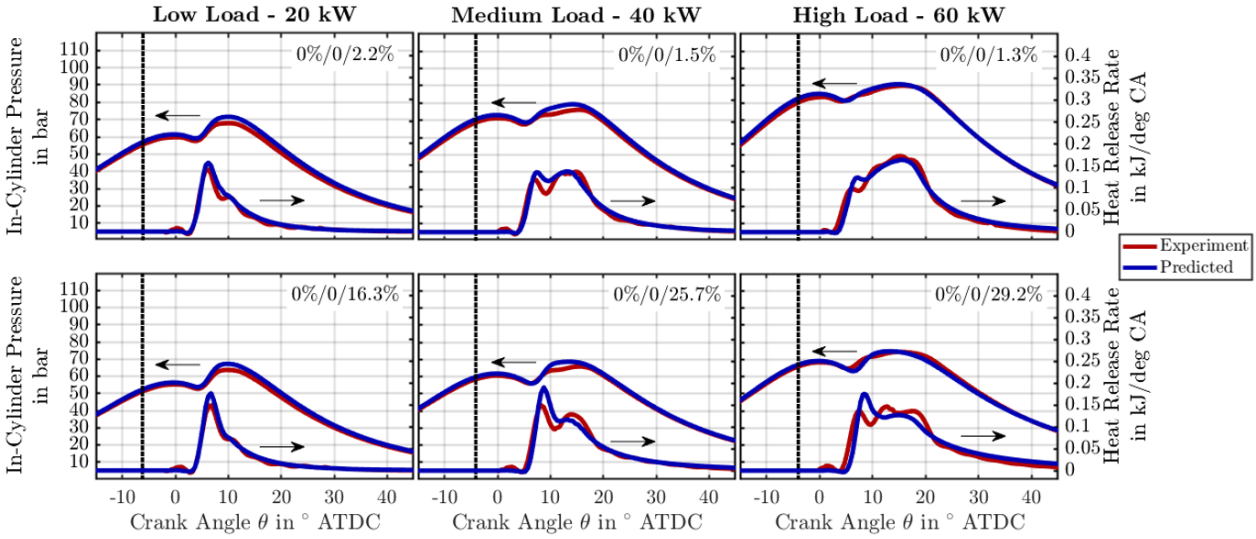

(a)

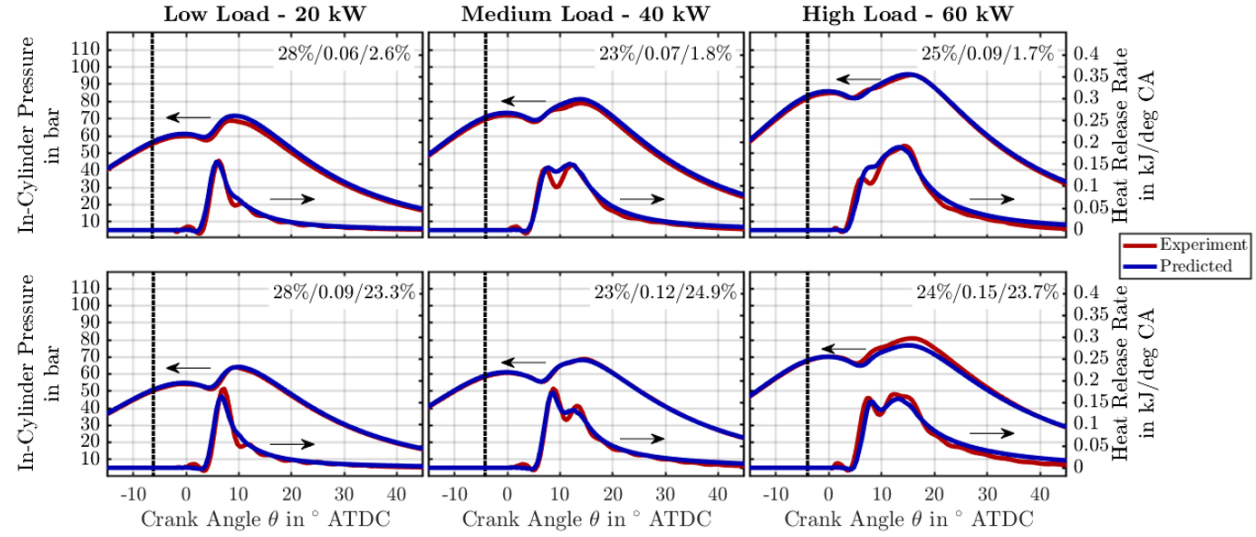

(b)

Figure 8: Comparison between experimental (blue curve) and predicted (red curve) in-cylinder pressure and heat release rate for (a) for diesel operation only and (b) medium hydrogen share ratio (up to 28 percent) and equivalence ratios beyond the flammability limit. The left column of graphs shows low (20 kW), the centre medium (40 kW) and the right column high (60kW) load cases and variations with no EGR results on top and cases with EGR on the bottom. The dashed vertical line marks the electrical signal for the main fuel injection. Annotations in the top right corner of each subplot show hydrogen energy share ratio/equivalence ratio/EGR rate.

peak pressure to around 1-4 percent. At higher loads the offset in SOC has reduced to 0.5 percent and while the change with respect to the low EGR case is minimal, the high EGR case, as shown in the bottom right corner of Figure 8b, experiences increased underprediction of in-cylinder pressure as a consequence of the late prediction of SOC and lower heat release rate compared to the diesel-only operation.

Further increasing hydrogen share ratio in turn leads to higher hydrogen-air equivalence ratios that can lie within the flammability limit of 0.2. This initiates flame propagation of the hydrogen mixture from which stems an increased heat release rate and thus higher in-cylinder pressure. The effect of this is presented in Figure 9. The graph depicts hydrogen share ratios of up to 57 percent and equivalence ratios varying between 0.14 and 0.29. Therefore, despite the high energy share ratio, all cases with low EGR rate (top row graphs in Figure 9) are below the flammability limit. These shall be discussed first in more detail. When comparing the experimental heat release rate and in-cylinder pressure without EGR across Fig. 8a- 9 it becomes apparent that both increase as hydrogen share ratio increases even though the mixture is too lean for flame propagation (Φ <0.2). This stems from the combustion of diesel and entrained hydrogen into the injected liquid fuel. For low to medium hydrogen share ratios of up to around 25 percent, the effect is still moderate and thus less obvious. However, comparing this with the simulation data shows that if hydrogen share

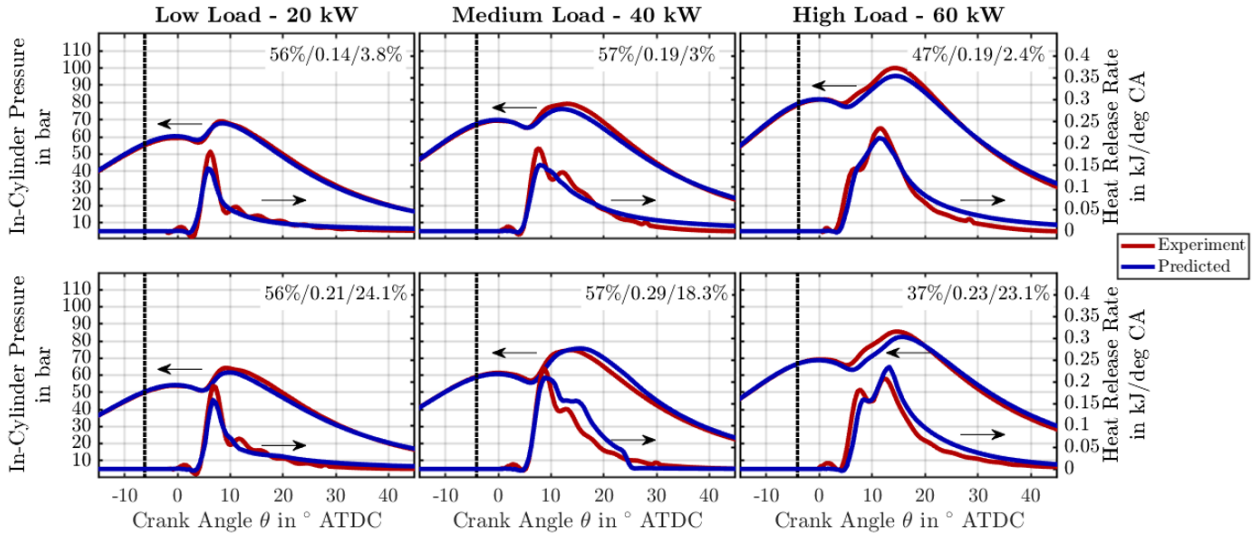

Figure 9: Comparison between experimental (blue curve) and predicted (red curve) in-cylinder pressure and heat release rate for medium hydrogen share ratio (up to 57 percent). Equivalence ratios vary between 0.14 and 0.29. The left column of graphs shows low (20 kW), the centre medium (40 kW) and the right column high (60kW) load cases and variations with no EGR results on top and cases with EGR on the bottom. The dashed vertical line marks the electrical signal for the main fuel injection. Annotations in the top right corner of each subplot show hydrogen energy share ratio/equivalence ratio/EGR rate.

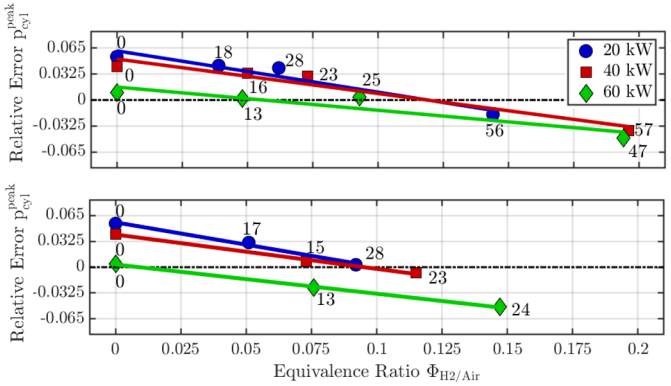

Figure 10: Relative error in peak pressure plotted against hydrogen-air equivalence ratio for cases without EGR (top) and with EGR (bottom). The numbers next to each data point denote the hydrogen share ratio in percent.

ratio is increased further- as done in Fig. 9- the entrainment and combustion of diesel and hydrogen is not accurately captured by the dual fuel model.

This trend is exemplified by Figure 10 that depicts the relative error in peak pressure between experiments and simulation as it varies with equivalence ratio and thus hydrogen content in the charge mixture. Initially, at zero hydrogen content within the charge mixture, peak pressures are overpredicted. As the hydrogen share is gradually increased, the error reduces linearly until the model starts underestimating peak pressures and thus peak heat release rates. In sum, this leads to relative errors in the range of approximately 5 percent. In light of the complex, three-dimensional nature of combustion processes such a level or accuracy is well within the acceptable range for one-dimensional modelling. However, it is important to notice that the model appears to struggle with the correct prediction of hydrogen entrainment. It is of course possible to re-calibrate the model by defining the entrainment multiplier as a function of hydrogen share ratio. However, this measure would significantly curb the model's predictive capabilities. It shall be noted that similar trends illustrated in Figure 10 can be witnessed when comparing heat release rates between experiments and simulation. Qualitatively, this can also be shown when comparing heat release rates between Figure 8b and 9. The higher the energy share ratio, the more the predicted heat release rate falls short off the experimentally determined one.

As soon as the hydrogen-air equivalence ratio is sufficiently high to foster flame propagation, as shown in the lower row of graphs in Figure 9, the model computes the laminar flame speed through Equation 5. The equivalence ratios are still close to the lower flammability limit yielding predicted flame speeds in the order of around 1-5 cm/s. Flame propagation is nonetheless sufficient to account for a marked increase in heat release rate and pressure, which is well captured by the model.

3.2. Double Injection

3.2.1. Diesel Operation

Double injections cases feature a pilot-injection of a small quantity of fuel prior to reaching top dead centre (TDC) and the main injection taking place just after TDC. For diesel-only cases, this results in the pressure and heat release rate distributions given in Figure 11a. Again, the top row denote results at different load cases without EGR rate, while the lower row of graphs yield results including EGR addition. In the absence of any hydrogen in the charge mixture, the heat release rate is characterised by a distinct two peak shape following pilot and main injection. There is satisfactory agreement between experimental and predicted heat release rate as well as in-cylinder pressure across all load cases and EGR rates. Nonetheless, the model consistently overestimates ignition delay for the pilot-injection as well as the amount of heat release in the process.

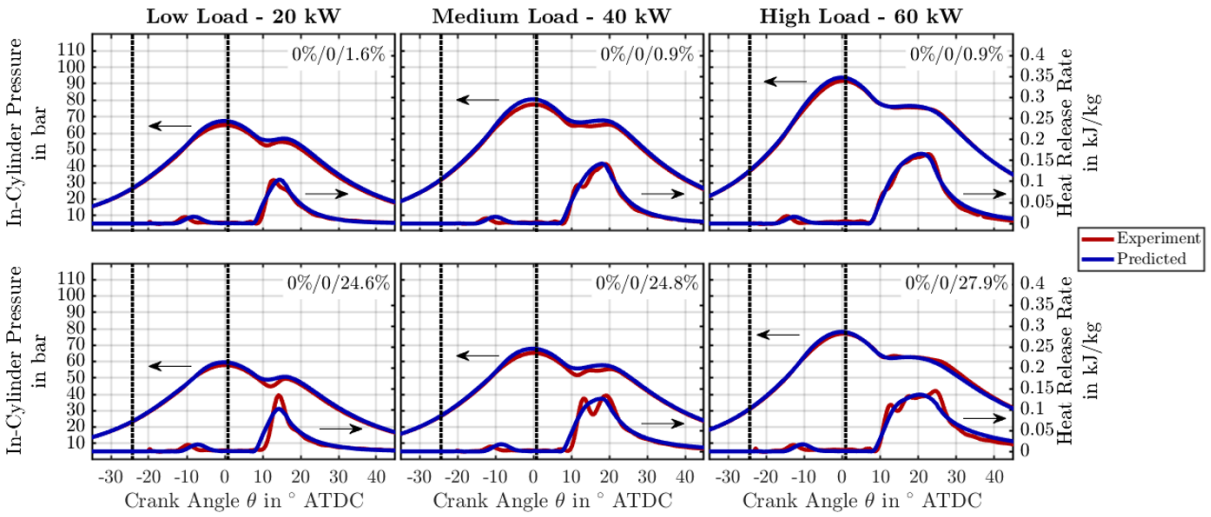

(a)

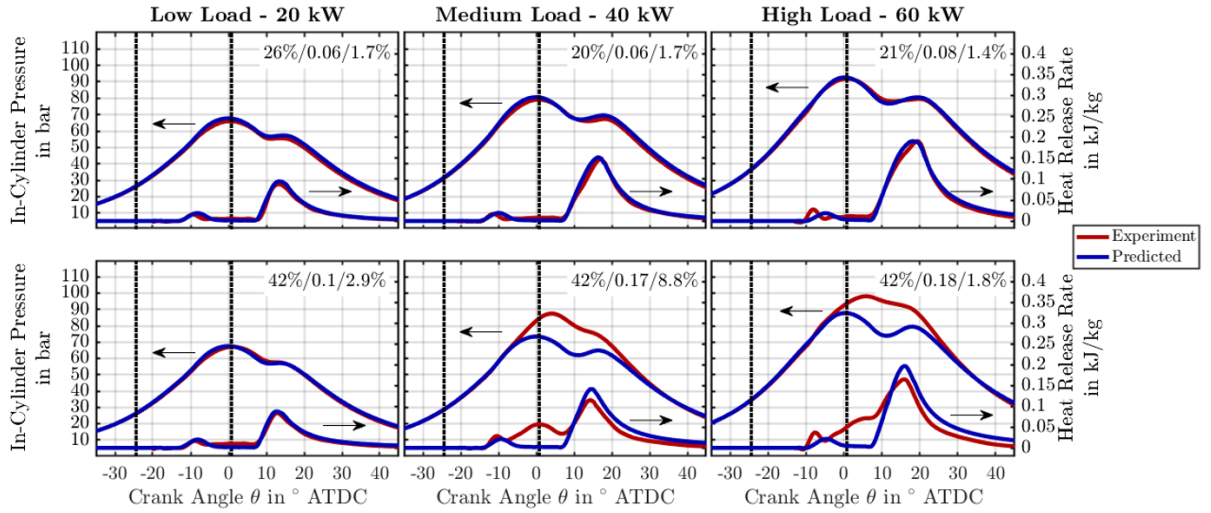

(b)

Figure 11: Comparison between experimental (blue curve) and predicted (red curve) in-cylinder pressure and heat release rate for (a) diesel operation and (b) medium hydrogen share ratio (up to 42 percent) with equivalence ratios beyond the flammability limit. The left column of graphs shows low (20 kW), the centre medium (40 kW) and the right column high (60kW) load cases and variations with no EGR results on top and cases with EGR on the bottom. The left dashed vertical line marks the electrical signal for the pilot fuel injection, while the right one denotes the signal for the main fuel injection. Annotations in the top right corner of each subplot show hydrogen energy share ratio/equivalence ratio/EGR rate.

The consequence is that the predicted peak cylinder pressure is by up to 4 percent larger than the experimentally one. A similar trend is witnessed by Piano et al. [21]. The calibration process seeks to minimise the error between measured and predicted heat release rate. It is thus not surprising that there will be larger deviations in the heat release rate for the pilot injection, since large deviations in the main injection heat release rate have a larger impact on overall error. The overprediction propagates further to the main injection, which then yields pressures that are in between 1-5 percent larger than in the experiments. This is slightly exacerbated by an early SOC present for all diesel-only cases. Nonetheless, MRE between experimental and predicted in-cylinder pressures range within 1.4 and 2.9 percent, as displayed in Table 5. In addition, despite the overestimated ignition delay for the pilot injection RMSE for heat release rates are only marginally larger compared to single Diesel injection cases.

Table 5: Mean relative error (MRE) for in-cylinder pressure and root mean squared errors (RMSE) for heat release rate between experiments and simulation for dual-injection diesel-only cases with and without EGR.

	20 kW	40 kW	60 kW
p_{cyl} MRE with EGR	2.1%	2.5%	1.8%
HRR RMSE with EGR	0.0065	0.0067	0.0075
p_{cyl} MRE w/o EGR	2.9%	2.5%	1.4%
HRR RMSE w/o EGR	0.0042	0.0044	0.0045

3.2.2. Hydrogen-Diesel Dual Fuel Operation

Initially, at low EGR rates and for hydrogen share ratios of approximately 20-26 percent, the introduction of hydrogen into the charge mixture does not alter the distinct two-peak heat release rate, as illustrated in Figure 11b. All cases encompass zero EGR. Equivalence ratio is well beyond the flammability limit ranging from 0.06 to 0.08. For all load cases both heat release rate and in-cylinder pressure are well captured. Similar to the conventional diesel operation, the initial peak in heat release rate originates from combustion of a small amount of diesel being injected during the compression stroke and hydrogen and air entrained in the spray plume. The second, larger peak stems from combustion of the main injection quantity and again entrains further hydrogen and air in the process. However, the experimental data reveals that as load is increased the heat release rate in between the two fuel injection pulses does not fully return to zero any more, while the simulation model maintains this trend and does not capture the change in behaviour as seen in the experiments. This is a relative subtle feature at lower hydrogen share ratios and appears to become more pronounced at higher load.

The situation becomes more clear when hydrogen share ratio is further increased to 42 percent. There is still no flame propagation expected, although equivalence ratios increase to a range of 0.1-0.18. Again, EGR rates remain zero, with the exception of the 40 kW, where a low EGR rate of approximately 9 percent was included. At low load conditions, the effect is still hardly noticeable, although there is a clear non-zero heat release rate in between pilot and main-injection. However, this continues to have little effect on the accuracy of the predicted in-cylinder pressure. Moving towards medium and high load cases, characteristics change substantially and significant discrepancies between model and experiments occur. The heat release profile shifts from the diesel-typical twin-peak shape towards a continuously increasing rate until main-injection takes place. The phenomenon takes place during the compression stroke and in conjunction with the ongoing compression this accounts for considerably larger in-cylinder pressures. As a result, one can observe a smearing of the two peaks in both heat release rate and in-cylinder pressure. The reason for the witnessed behaviour stems presumably from the higher hydrogen content in the cylinder charge that is entrained within the diesel pilot-jet and is ignited along with the liquid fuel as the cylinder moves upwards towards TDC. While, the simulation model was able to predict combustion performance in single-injections reasonably well, it cannot capture the effects of double-injection at medium and higher loads and continues to reflect the distinct diesel two-peak profiles. Since the main effects associated with this occur during the compression stroke, the shortcomings of the multi-zone combustion models with respect to flow entrainment become more pronounced and larger differences in the predicted characteristics transpire.

4. Conclusions and Outlook

The focus of this study is on the capacity of widely used predictive multi-zone combustion models in one-dimensional engine performance simulations. The study employed the dual-fuel combustion model implemented in GT-Power in combination with a laminar flame speed fitting model derived from one-dimensional, freely propagating flame simulations in Chemkin. The performance and limitations of the simulation model with respect to experimental data was then examined over a range of engine loads, hydrogen share ratios, equivalence ratios and EGR rates and for two different injection strategies. The conclusions drawn from the study can thus be summarised as follows:

- Current version of GT-Power (v2019) necessitates a user-defined model that computes laminar flame speed instantaneously based on hydrogen/air equivalence ratio, in-cylinder pressure, unburned zone temperature and residual mass fraction. The model proposed in this study yields flame speeds in good agreement with data from the literature and proves to exhibit satisfactory performance when applied to the predictive combustion model in GT-Power.

- For single diesel injection the model is able to capture the effects of hydrogen addition in the charge mixture well. This holds for hydrogen share ratios up to 57 percent and hydrogen/air equivalence ratios of up to 0.29. However, there is a clear, discernible trend toward underprediction of hydrogen entrained within the injected diesel spray leading to heat release rates and in-cylinder pressures that fall below what is witnessed during the laboratory tests.

- The trend indicated by the single-injection study appears to be further aggravated when a double-injection strategy is taken. The model is able to reproduce the experimental data up to a hydrogen share ratio of up to 26 percent. However, at higher share ratios, the model cannot capture partial hydrogen combustion initiated by pre-injection. Under these circumstances, the model erroneously maintains a distinct two-peak heat release rate distribution.

- Given the performance benefit of the hydrogen-diesel dual fuel engine and its potential to mitigate carbon footprint of internal combustion engines in the short and medium term, there is a clear need for further research on modelling of hydrogen-diesel dual fuel combustion.

Acknowledgement

The financial support of the Daiwa Anglo-Japanese Foundation and the Great Britain Sasakawa Foundation is highly appreciated. The authors would also like to thank Kevin Roggendorf and Jared Cromas from Gamma Technologies for their invaluable help and suggestions during the modelling campaign.

References

[1] B.J. Bora, U.K. Saha, S. Chatterjee and V. Veer, Effect of compression ratio on performance, combustion and emission characteristics of a dual fuel diesel engine run on raw biogas, Energy Conversion and Management 87 (2014) 1000 – 1009.

[2] P. Dimitriou and T. Tsujimura, A review of hydrogen as a compression ignition engine fuel, International Journal of Hydrogen Energy 42 (2017) 24470 – 24486.

[3] P. Dimitriou, T. Tsujimura and Y. Suzuki, Low-load hydrogen-diesel dual-fuel engine operation - A combustion efficiency improvement approach, International Journal of Hydrogen Energy (2019) https://doi.org/10.1016/j.ijhydene.2018.05.062.

[4] S. Nag, P. Sharma, A. Gupta and A. Dhar, Experimental study of engine performance and emissions for hydrogen diesel dual fuel engine with exhaust gas recirculation, International Journal of Hydrogen Energy 44 (2019) 12163 – 12175.

[5] P. Dimitriou, M. Kumar, T. Tsujimura and Y. Suzuki, Combustion and emission characteristics of a hydrogen-diesel dual-fuel engine, International Journal of Hydrogen Energy 43 (2018) 13605 – 13617.

[6] P. Dimitriou, T. Tsujimura and Y. Suzuki, Adopting biodiesel as an indirect way to reduce the NOx emission of a hydrogen fumigated dual-fuel engine, Fuel 244 (2019) 324–334.

[7] T. Tsujimura and Y. Suzuki, The utilization of hydrogen in hydrogen/diesel dual fuel engine, International Journal of Hydrogen Energy 42 (2017) 14019 – 14029.

[8] M. Deb, G.R.K. Sastry, R.S. Panua R. Banerjee and P.K.Bose, Effect of Hydrogen-Diesel Dual Fuel Combustion on the Performance and Emission Characteristics of a Four Stroke-Single cylinder Diesel Engine, International Journal of Mechanical, Aerospace, Industrial, Mechatronic and Manufacturing Engineering 9 (2015) 914 – 920.

[9] M. Talibi, P. Hellier and N. Ladommatos, The effect of varying EGR and intake air boost on hydrogen-diesel co-combustion in CI engines, International Journal of Hydrogen Energy 42 (2017) 6369 – 6383.

[10] G. Li, X. Yu, W. Shi, C. Yao, S. Wang and Q. Shen, Effects of split injection proportion and the second injection timings on the combustion and emissions of a dual fuel SI engine with split hydrogen direct injection, International Journal of Hydrogen Energy 44 (2019) 11194–11204.

[11] I.M.M. Elsemary, A.A.A. Attia, K.H. Elnagar and M.S. Elsaleh, Spark timing effect on performance of gasoline engine fueled with mixture of hydrogengasoline, International Journal of Hydrogen Energy 42 (2017) 30813 – 30820.

[12] R. Niu, X. Yu, Y. Du, H. Xie, H. Wu and Y. Sun, Effect of hydrogen proportion on lean burn performance of a dual fuel SI engine using hydrogen direct-injection, Fuel 186 (2016) 792–799.

[13] H. Wu, X. Yu, Y. Du, X. Ji, R. Niu, Y. Sun and J. Gu, Study on cold start characteristics of dual fuel SI engine with hydrogen direct-injection, Applied Thermal Engineering 100 (2016) 829 – 839.

[14] A. Menaa, M.S. Lounici, F. Amrouche, K. Loubar and M. Kessal, CFD analysis of hydrogen injection pressure and valve profile law effects on backfire and pre-ignition phenomena in hydrogen-diesel dual fuel engine, International Journal of Hydrogen Energy 44 (2019) 9408 – 9422.

[15] O.H. Ghazal, Combustion simulation of direct injection CI engine operating on dual fuel using CFD, Acta Physica Polonica A 134 (2018) 387–390.

[16] P. Sharma and A. Dhar, Compression ratio influence on combustion and emissions characteristic of hydrogen diesel dual fuel CI engine: Numerical Study, Fuel 222 (2018) 852–858.

[17] W.B. Santoso, R.A. Bakar and A. Nur, Combustion Characteristics of Diesel-Hydrogen Dual Fuel Engine at Low Load, Energy Procedia 32 (2013) 3 – 10. International Conference on Sustainable Energy Engineering and Application (ICSEEA) 2012.

[18] V. Chintala and K.A. Subramanian, CFD analysis on effect of localized in-cylinder temperature on nitric oxide (NO) emission in a compression ignition engine under hydrogen-diesel dual-fuel mode, Energy 116 (2016) 470 – 488.

[19] H. Koten, Hydrogen effects on the diesel engine performance and emissions, International Journal of Hydrogen Energy 43 (2018) 10511 – 10519.

[20] J. Hvezda, Multi-Zone Models of Combustion and Heat Transfer Processes in SI Engines, in: SAE 2014 World Congress Exhibition, SAE International, 2014.

[21] A. Piano, F. Millo, G. Boccardo, M. Rafigh, A. Gallone and M. Rimondi, Assessment of the Predictive Capabilities of a Combustion Model for a Modern Common Rail Automotive Diesel Engine, in: SAE 2016 World Congress and Exhibition, SAE International, 2016.

[22] O.H. Ghazal, Combustion analysis of hydrogen-diesel dual fuel engine with water injection technique, Case Studies in Thermal Engineering 13 (2019) 100380.

[23] E. Monemian, Simulating Diesel-Hydrogen Combustion by GT-Power, Proceedings of the FISITA World Automotive Congress (2018).

[24] K.T. Aung, M.I. Hassan and G.M. Faeth, Flame stretch interactions of laminar premixed hydrogen/air flames at normal temperature and pressure, Combustion and Flame 109 (1997).

[25] M. Berman, Sandia Laboratories Report, Technical Report, SSAND84-0689, S1984.

[26] Y.Dong, A.T. Holley, M.G. Andac, F.N. Egolfopoulos, S.G. Davis, P. Middha and H. Wange, Extinction of premixed H_2/air flames: Chemical kinetics and molecular diffusion effects, Combustion and Flame 142 (2005) 374–387.

[27] D.R. Dowdy, D.B. Smith, S.C. Taylor and A. Williams, The use of expanding spherical flames to determine burning velocities and stretch effects in hydrogenair mixtures, Symposium (International) on Combustion 23 (1991) 325–332. Twenty-Third Symposium (International) on Combustion.

[28] F.N. Egolfopoulos and C.K. Law, An experimental and computational study of the burning rates of ultra-lean to moderately rich H2/O2/N2 laminar flames with pressure variations, Symposium (International) on Combustion 23 (1991) 333–340.

[29] R. Günther and G. Janisch, Measurements of burning velocity in a flat flame front, Combustion and Flame 19 (1972) 49–53.

[30] T. Iijima and T. Takeno, Effects of temperature and pressure on burning velocity, Combustion and Flame 12 (1986) 445–452.

[31] G.W. Koroll, R.K. Kumar and E.M. Bowles, Burning velocities of hydrogenair mixtures, Combustion and Flame 94 (1993) 330–340.

[32] M.C. Krejci, O. Mathieu, A.J. Vissotski, S. Ravi, T.G. Sikes, E.L. Petersen, A. Kérmonès, W. Metcalfe and H.J. Curran, Laminar Flame Speed and Ignition Delay Time Data for the Kinetic Modeling of Hydrogen and Syngas Fuel Blends, J. Eng. Gas Turbines Power 135 (2012).

[33] O.C. Kwon, L.-K. Tseng and G.M. Faeth, Laminar burning velocities and transition to unstable flames in H2/O2/N2 and C2H8/O2/N2 mixtures, Combustion and Flame 90 (1992) 230–246.

[34] D.D.S. Liu and R. MacFarlane, Laminar burning velocities of hydrogen-air and hydrogen-air-steam flames, Combustion and Flame 49 (1983) 59–71.

[35] J. Pareja, H.J. Burbano and Y. Ogami, Measurements of the laminar burning velocity of hydrogenair premixed flames, International Journal of Hydrogen Energy 35 (2010) 1812–1818.

[36] K.T. Aung, M.I. Hassan and G.M. Faeth, Flame stretch interactions of laminar premixed hydrogen/air flames at normal temperature and pressure, Combustion and Flame 109 (1997).

[37] F. Takahashi, M. Mizomoto and S. Ikai, Laminar burning velocities of hydrogen/oxygen/inert gas mixtures, Alternative Energy Sources III 5 (1983) 447–457.

[38] S.D. Tse, D.L. Zhu and C.K. Law, Morphology and burning rates of expanding spherical flames in H2/O2/inert mixtures up to 60 atmospheres, Proceedings of the Combustion Institute 28 (2000) 1793 – 1800.

[39] C.M. Vagelopoulos, F.N. Egolfopoulos and C.K. Law, Further considerations on the determination of laminar flame speeds with the counterflow twin-flame technique, Symposium (International) on Combustion 25 (1994) 1341–1347.

[40] C.K. Wu and C.K Law, On the determination of laminar flame speeds from stretched flames, Symposium (International) on Combustion 20 (1985) 1941 – 1949. Twentieth Symposium (International) on Combustion.

[41] E. Varea, J. Beeckmann, H. Pitsch, Z. Chen and B. Renou, Determination of burning velocities from spherically expanding H_2/air flames, Combustion and Flame 35 (2015) 711–719.

[42] O. Park, P.S. Veloo, H. Burbano and F.N. Egolfopoulos, Studies of premixed and non-premixed hydrogen flames, Combustion and Flame 162 (2015) 1078–1094.

[43] N. Lamoureux, N. Djebaili-Chaumeix and C.E. Paillard, Laminar flame velocity determination for H2airsteam mixtures using the spherical bomb method, Journal de Physique de France IV 109 (2002).

[44] A.K. Das, K. Kumar and C.J. Sung, Laminar flame speeds of moist syngas mixtures, Combustion and Flame 158 (2011) 345–353.

[45] N.M. Marinov, C.K. Westbrook and W.J. Pitz, Detailed and global chemical kinetics model for hydrogen, Transport Phenomena in Combustion 1

(1996).

[46] V.A. Alekseev, M. Christensen, E. Berrocal, E.J.K. Nilsson and A.A. Konnov, Laminar premixed flat non-stretched lean flames of hydrogen in air, Combustion and Flame 162 (2015) 4063–4074.

[47] E. Hu, Z. Huang, J. He and H. Miao, Experimental and numerical study on laminar burning velocities and flame instabilities of hydrogenair mixtures at elevated pressures and temperatures, International Journal of Hydrogen Energy 34 (2009) 8741–8755.

[48] S. Verhelst, R. Woolley, M. Lawes and R. Sierens, Laminar and unstable burning velocities and Markstein lengths of hydrogenair mixtures at engine-like conditions, Proceedings of the Combustion Institute 30 (2005) 209–216.

[49] V.A. Alekseev, M. Christensen and A.A. Konnov, The effect of temperature on the adiabatic burning velocities of diluted hydrogen flames: A kinetic study using an updated mechanism, Combustion and Flame 162 (2015) 1884–1898.

[50] J Kee, R and F Grcar, J and D Smooke, M and A Miller, J and Meeks, Ellen, PREMIX: a fortran program for modeling steady laminar one-dimensional premixed flames, Sandia Rep 143 (1985) .

[51] G. P. Smith, D. M. Golden, M. Frenklach, N. W. Moriarty, B. Eiteneer, M. Goldenberg, C. T. Bowman, R. K. Hanson, S. Song, W. C. Gardiner, Jr., V. V. Lissianski, and Z. Qin, GRI-Mech 3.0, The Gas Research Institute. URL `http://www.me.berkeley.edu/gri mech/+`.

[52] J.B. Heywood, Internal Combustion Engine Fundamentals, McGraw-Hill, New York, 1988.